Stability analysis of high speed lab centrifuges considering internal damping in rotor-shaft joints

J. Fischer, J. Strackeljan

Rotors of high speed lab centrifuges are often removable to enable the use of different rotors for one single drive. The removable rotor shaft connection is the main reason for internal damping leading to self excited vibrations. In this paper different models of internal damping are investigated. The main influence parameters for stability are deduced analytically and numerically. The numerical simulations were carried out with the simulation tool FERAN. It was developed by the authors and is introduced in this paper. The primarily objective of the paper is to demonstrate instability effects which could occur in real lab centrifuges and which could be hardly simulated by a simple 4 or 8 degree of freedom model of a Jeffcot rotor.

1 Introduction

Advanced high speed laboratory centrifuges are designed as universal devices where one motor drives a wide range of different rotors (figure 1, left). Large-volume rotors with masses up to $20\,kg$, for particular blood centrifuges even $60\,kg$ are used in laboratories. In general a high speed centrifuge operates with speeds up to $30000\,rpm$ and centrifuge drive systems operate below and above critical speeds. Below critical speeds, the centrifuge rotor rotates about its geometric center. Above the critical speeds, the centrifuge rotor attempts to rotate about its mass center.

In the design of high speed rotors comfort and safety have to be considered from the beginning of the design process. Efforts are undertaken to obtain a huge tolerance of unbalance for avoiding time consuming taring of samples. Auto-balancing devices or drive concepts, where the mechanical design allows high unbalances are possible solutions(Ryzhik et al. (2004)).
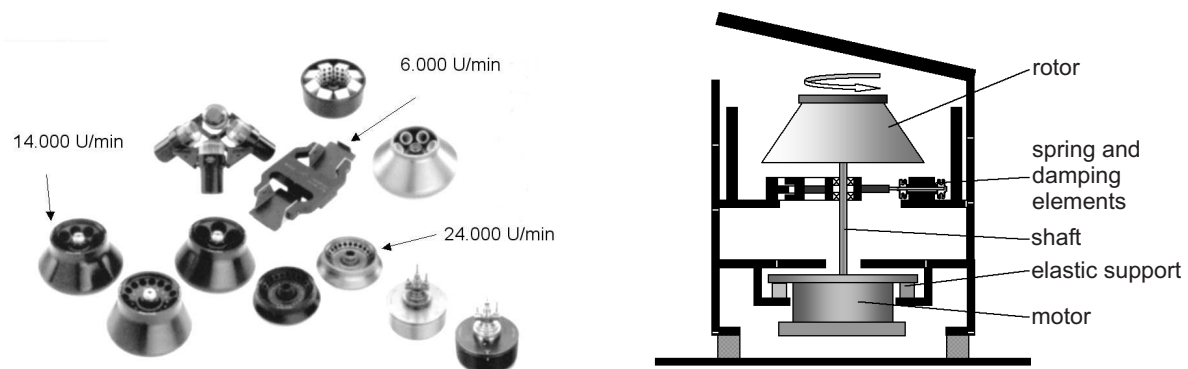

Figure 1: Rotors of an advanced lab centrifuge(left) Needle centrifuge (right)

7.5 Another focus of recent developments is the problem of instable rotor behavior due to internal damping. This kind of stability problems have been studied for many years from a theoretical point of view (Kellenberger (1963), Hagedorn et al. (1977), Schäfer (1994)). Most of the problems are well known but the operating conditions for most laboratory centrifuges did not exceed stability limits. But with the increase of operating speed a couple of serious accidents occurred during the last years. The main reason for the internal damping effects is that lab centrifuges systems typically use a removable rotor for holding sample containers which contain the sample to be separated. The effects of internal damping and friction between rotating parts, which occurs when rotating parts are slackly attached to each other can provoke self excited vibrations. As shown in Figure 1 the shaft connects the

drive motor and the rotor. It often takes the form of a thin needle. When designing a shaft for a rotor assembly used in a centrifuge the design objectives are usually in conflict. One objective is to have a very flexible shaft in order to minimize bearing load at super critical speeds. A second objective is to minimize the rotor displacement at the critical speed. In conventional designs the shaft diameter is usually chosen as a compromise between these two competitive objectives. Smaller diameter shafts also limit the amount of torque that can be transmitted, thus limiting the acceleration rate. The disadvantage of a thin needle as a shaft is the lack of control possibility by external design elements like dampers and springs. Therefore it is necessary to support the needle by bearings (Figure 1).

Figure 2 shows the horizontal rotor acceleration of a centrifuge which gets unstable because of internal damping. The vibrations increases in less than 1 s to a level which leads to a serious damage of the centrifuge and the sensor system. In this case the vibration occurs with the frequency of the forward whirl, which is the closest one to the frequency of the rotational frequency (Figure 2, right). Due to the fact that most lab centrifuges do not feature any active elements like magnetic bearings, the control of this instability is hardly possible. In consequence the design of a drive should avoid this situation in any circumstance.
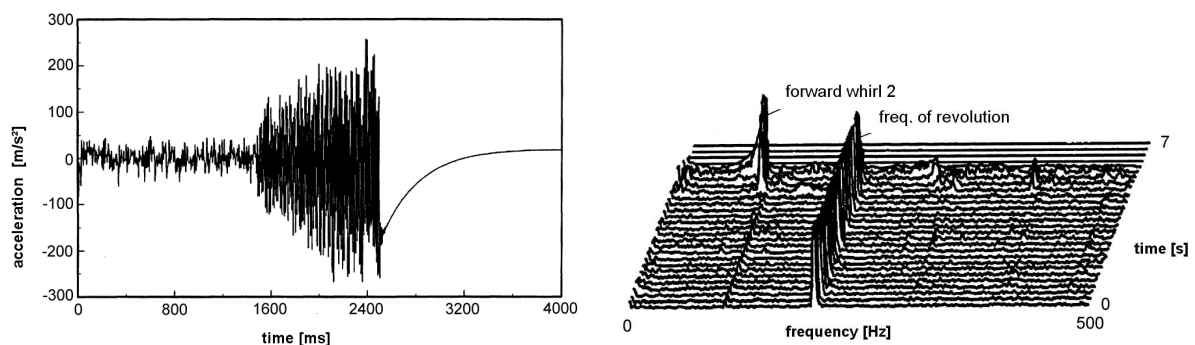

Figure 2: Rotor acceleration of a centrifuge getting unstable due to internal damping

Therefore the development of new concepts for high speed centrifuges and the improvement of existing systems require simulation tools which offer the possibility of special adaptation. Over a couple of years the authors use the simulation tool LUBEST for related design and optimization tasks (Strackeljan et al. (2001), Feng (2002)). Even if no internal damping was considered the prediction of the remaining system damping allows a reasonable statement about the stability. If the internal damping parameter could not be determined by experiments or theoretical studies with an acceptable accuracy the solution of the simulation will offer a high degree of uncertainty. Unfortunately it is very difficult to describe the physics behind the phenomenon of internal damping of rotor shaft assemblies.

In this paper the authors present the FEM program FERAN, which was developed during the last years at the Universities Clausthal and Magdeburg. It is well suited to determine eigenvalues, oscillations, stresses, and bearing loads of rotor systems (Fischer and Strackeljan (2005), Fischer and Strackeljan (2006)). Due to the open program code, FERAN can be linked with algorithms to conduct automated parameter studies or optimization. Rotor systems are governed by many parameters like bearing stiffness and damping, the length and width of the shaft and the moments of inertia, which can be altered to enhance the dynamic properties.

In Section 3 two different Jeffcott Rotors with internal damping are investigated analytically to Figure out the main influence parameters to the range of stability. In addition the simulation results of high speed centrifuges with linear viscous internal damping in rotor shaft connections are presented. A viscous internal damping model is appropriate if rubber elements are introduced in the joint of rotor and shaft. They are used to facilitate the change of rotors or to uncouple rotor and shaft movements in the post critical speed range.

Nonlinearities in rotor systems are caused, e.g., by clearance in ball bearings (Irretier (2001)), oil films in a journal bearing or dry friction between the shaft and mounted elements. Some of these nonlinearities can be included in the dynamic simulation by FERAN. Dry friction is such a nonlinearity, which is discussed later on. Internal dry friction fits more to the micro-movements which occur between shaft and rotor, if no rubber elements are used. One model for internal dry friction is studied on a Jeffcott Rotor. The simulation results are included.

2 Theoretical background

In the following the theoretical background of the FEM-software FERAN which is coded in C++ will be presented only compendiously.

2.1 The fundamental equations

The dynamic behavior of a rotor system is described by the discrete differential equation in the inertial coordinate system.

$$[M]\{\ddot{D}\} + [[C] + [G]]\{\dot{D}\} + [K]\{D\} = \{F^{ext}\} + \{F^{nl}\} \tag{1}$$

with stiffness matrix $[K]$, damping matrix $[C]$, gyroscopic matrix $[G]$ and mass matrix $[M]$. Vector $\{D\}$ consists of the nodal displacements, vector $\{F^{ext}\}$ of the linear external, and $\{F^{nl}\}$ of the non-linear internal and external forces. To obtain equation (1), the principle of linear momentum is first stated in a body fixed coordinate system and subsequently transformed into the inertial coordinate system. The internal forces $\{F^{int}\} = [K] \cdot \{D\}$ in a coordinate system rotating with the frequency of revolution are transformed into the inertial coordinate system.

The shaft of the rotor system is discretised by beam elements, including transverse shear deformation optionally, according to Timoshenko's beam theory (Cowper (1966)). Beam elements can reflect deformations due to bending loads, torque loads, and axial forces. The mass properties of the beam elements are described by a consistent mass matrix. For the gyroscopical matrix a lumped approach is used.

2.2 Boundary conditions and constraints

Each node of the used beam element consists of 6 degrees of freedom. If the degrees of freedom of any node represent motions, which are prevented by supports, the corresponding rows and columns in the global matrices have to be eliminated. The developed FEM-software can take into account different bearings with different stiffness and damping properties. At each node of the shaft, three spring elements and three dampers in each rotational and translational direction can be included. The upper and lower shaft bearing of centrifuges are often coupled rigidly by the stator. Under consideration of constraints, which connect the movements of the corresponding nodes, the behavior of the stator can be simulated.

2.3 Calculation of eigenvalues

As an approach for the homogenous solution of the differential equation (1), the function

$$\{D_h(t)\} = \{\hat{D}_h\} \cdot e^{pt} \tag{2}$$

is chosen. By introducing this into equation (1) and with some calculations we obtain the standard eigenproblem

$$([K_U] - p \cdot [I])\{\hat{D}_U\} = \{0\} \tag{3}$$

with the unit matrix $[I]$. The matrix $[K_U]$ is an asymmetrical matrix. During the last years, different solvers for eigenproblems have been developed, like the Jacobian method, the Householder-QR method, the determinant search method, the Sturm sequence, the inverse iteration, or the Lanzcos method. The suitability of an algorithm for a given task depends on the size and structure of the matrices, the numbers of eigenvalues which should be considered, and how skilfully algorithms are coded. As the rotor system is described by few elements, the arrays of the eigenproblem are comparative small. Thus a method which calculates all eigenpairs can be used. The matrix $[K_U]$ is asymmetric. Hence the application of the Householder-QR method is expedient. In FERAN a readily modified Householder-QR algorithm of Wilkinson and Reinsch (1971) is implemented.

2.4 Steady state calculation of deflections, forces and stresses

In the steady state case one considers vibrations that continue at constant amplitude and at the frequencies of the force function after initial transients have disappeared because of damping. To compute this harmonic response of the rotor system, an unbalance load $\{F_i^{ext}(t)\} = \{\hat{F}_i^{ext}\} \cdot e^{j\Omega t}$ with constant speed of revolution Ω is applied to

the structure at node i. The load is split in the real and imaginary part. Assuming $\{D_p(t)\} = \{\hat{D}_p\} \cdot e^{pt}$ as solution for the inhomogeneous part of the linear equation of motion (1), one gets

$$[\hat{K}(j\Omega)]\{\hat{D}_p\} = \{\hat{F}\}. \tag{4}$$

$[\hat{K}(j\Omega)]$ is the complex dynamic stiffness matrix. By separating the imaginary and real part, a system of equations is computed, which can be solved by a Gauss algorithm (Schwarz (1993)). Nonlinearities can not be considered by this calculation. Forces are computed by equation (4), whereby rows and columns deleted due to boundary conditions have to be added to the complex dynamic stiffness matrix $[\hat{K}(j\Omega)]$. The calculation of stresses is carried out regarding the continuous deformations according to the basic theories of torsion, beams and bars.

2.5   Numerical integration of the equations of motion

The response history of a rotor-system due to unbalance loads can be calculated by direct time integration methods using finite difference approximations of time derivatives. In FERAN different explicit and implicit methods are applied. The trapezoidal rule is used in FERAN as an implicit method (Cook et al. (2002)). This method is unconditional stable, but it can not be used for nonlinear systems unless in each step the nonlinear equation

$$[K^{eff}]_{n+1} \cdot \{D\}_{n+1} - \{F^{nl}(\{D\}_{n+1})\} = h(\{D\}_n, \{\dot{D}\}_n, \{\ddot{D}\}_n) \tag{5}$$

is solved by a Newton algorithm to obtain $\{D\}_{n+1}$. The matrix $[K^{eff}]$ consists of

$$[K^{eff}]_{n+1} = \frac{1}{\beta \cdot \Delta t^2}[M]_{n+1} + \frac{\gamma}{\beta \cdot \Delta t}[C]_{n+1} + [K]_{n+1} \tag{6}$$

and $h(\{D\}_n, \{\dot{D}\}_n, \{\ddot{D}\}_n)$ is a function depending on the degrees of freedom of time step n, the matrices $[C]_{n+1}$ and $[M]_{n+1}$ and the external linear force vector $\{f^{ext}\}_{n+1}$ at time step $n + 1$.

The 3rd order Runge-Kutta method used in FERAN is suited to solve nonlinear problems but the solution becomes unstable, if the structure has huge eigenfrequencies even if Runge-Kutta methods of higher order are used. As a simple rule, time steps used for calculation should not exceed $\Delta t = T/\pi$, with $1/T$ the uppermost eigenfrequency.

In the presence of huge eigenvalues, the system of differential equations is stiff. Efficient integration methods for stiff problems should be implicit in character to obtain the required stability properties. Beneath implicit-direct-integration methods, modified Rosenbrock methods can be used. They are best suited when the differential equation of motion is nonlinear, since the Newton iteration in each step to solve equation (5) is avoided. Equation (1) can be expressed as

$$\{\dot{X}\} = \{f(\{X\})\}, \quad \{X\} = \{ \ \{D\} \quad \{\dot{D}\} \ \}^T \tag{7}$$

Basically the right side of the differential equation (7) is split in a linearisation and a small residue:

$$\{\dot{X}\} = [J(\{X\})] \cdot \{X\} + \left(\{f(\{X\})\} - [J(\{X\})] \cdot \{X\} \right). \tag{8}$$

The linear part is integrated implicitly. The small nonlinear residue in the huge brackets is integrated explicitly (Voss (2005)). The j-th column of the Jacobian matrix $[J(\{X\}]$ is computed by

$$\{J_j(\{X\})\} = \frac{1}{\delta}[\{f(\{X\} + \delta \cdot \{e_j\})\} - \{f(\{X\})\}. \tag{9}$$

Vector $\{e_j\}$ represents the j-th unit vector. Factor δ is arbitrary small.

Algorithms used in FERAN are a linear implicit 2nd order Runge-Kutta method introduced in Steihaug and Wolfbrandt (1979), and a linear implicit 2nd and 3rd order Runge-Kutta method with step control. The latter one is coded such that the Jacobian matrix is only recomputed in a time step if the error is higher than a certain boundary value.

2.6   Example: Simulation of a high speed lab centrifuge with FERAN

At the Institute of Applied Mechanics, University Magdeburg, measurements have been carried out on different high speed centrifuges. In addition, these centrifuges have been simulated by the developed software FERAN. The results for one of those centrifuges are presented in the following.
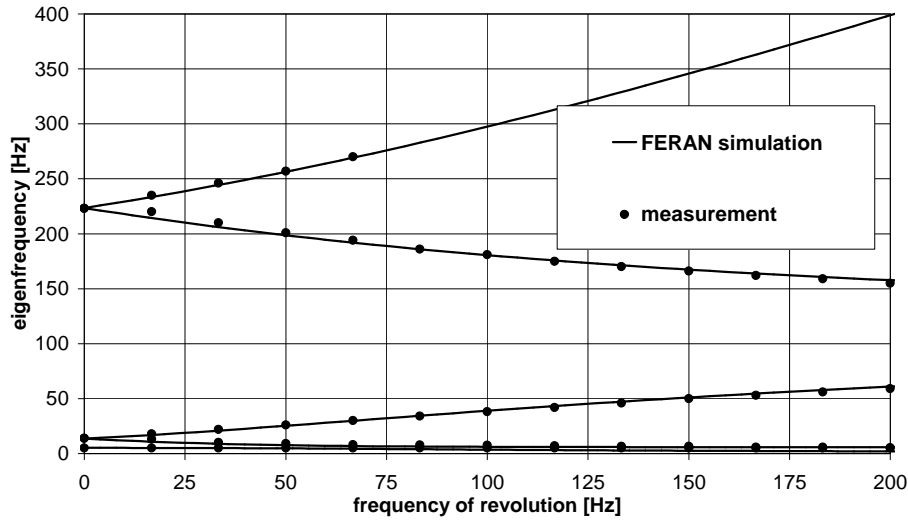
Figure 3: Campbell diagram of the high speed centrifuge. Simulation results of FERAN in comparison with measurement values.

The measured eigenvalues coincide well with the simulation results of FERAN (Figure 3). In the simulation model the connection between roller bearing and shaft is considered to be stiff. In reality, the shaft bearing connection is softer. To take into account the effects of the actual softer connection, the shaft diameter has to be reduced in the simulation model with respect to the original diameter. Regarding the high speed lab centrifuge, a shaft diameter reduction of 15 % leads to a good compliance between measurement and simulation results.
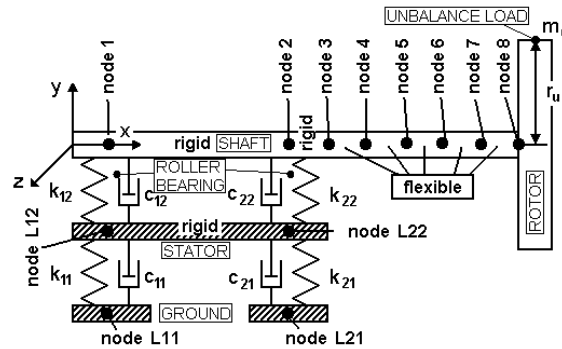

Figure 4: FEM-simulation model of a high speed centrifuge.

Figure 4 shows the FEM-simulation model of the centrifuge. The shaft is modelled by seven elements. The rigid rotor is attached to node 8 as well as the mass of unbalance m_u with radius of unbalance r_u. The bearing nodes $L12$ and $L22$ are connected with constraints. They represent the stator. The spring elements k_{12} and k_{22} and the damping elements c_{12} and c_{22} specify the properties of the roller bearings. The rubber support of the stator is modelled by two torsion springs. In Figure 4, only one of them, the torsion spring k_{11} is displayed. Furthermore, damping properties are taken into account by additional damping elements.

The parameters used for the simulation are: shaft diameter $20\,mm$ between node 1 and 2, $13\,mm$ between node 2 and node 7 and $22\,mm$ between node 7 and 8, shaft length $98\,mm$ ($68\,mm$ between node 1 and 2). Rotor: axial moment of inertia $J_{AS} = 0.0063\,kgm^2$, polar moment of inertia $J_{PS} = 0.0104\,kgm^2$ (both in respect to node 8), mass $m_S = 1.93\,kg$. Stator: moments of inertia $J_{PStator} = J_{AStator} = 0.01\,kgm^2$, mass $m_{Stator} = 5\,kg$. Rubber support: stiffness $k_{11t} = 9000\,N/m$ (translation), $k_{11r} = 180\,Nm$ (rotation), damping $c_{11t} = 75\,N{\cdot}s/m$, $c_{11r} = 0.06\,Nms$, $k_{21t} = 150\,N/m$. Roller bearings: $k_{12t} = k_{22t} = 60 \cdot 10^3\,N/m$. Unbalance load: mass $m_u = 0.003\,kg$ radius $r_u = 80\,mm$.

The high speed centrifuge which was object of our research work is offered by the manufacturer with a wide range of different rotors. Once the model is created in FERAN, the behavior of each rotor can be computed with minor

expense. Furthermore the effects of varying the geometrical, stiffness and damping properties of the centrifuge can be studied easily.

3 Viscous internal damping in rotor-shaft joints

Viscous internal damping is the easiest way to describe energy dissipation in rotor dynamics. It is commonly used to characterize damping of fluids or viscous dampers.

Prior to examine the implementation of viscous internal damping in the simulation of high speed centrifuges, we first analyze a Jeffcott Rotor with different models of viscous internal damping in order to identify the main parameters influencing the area of stability.

3.1 Two degrees of freedom Jeffcott rotor considering internal damping in the shaft

If material damping in the shaft of a two degrees of freedom Jeffcott Rotor is small enough, it can be approximately represented by viscous damping. The viscous internal damping is proportionally to the speed of deflection in the rotating coordinate system.

It is possible to calculate the eigenvalues of this system analytically. The system is stable if the real part of all eigenvalues is negative. By some basic assumption one obtains as boundary frequency $w_b = 1 + \frac{\vartheta_a}{\vartheta_i}$ (Gasch et al. (2002)). The boundary frequency w_b depends only on the ratio of internal and outer damping. For frequencies higher than w_b instability could occur.

The dimensionless frequency w is defined as $w = \frac{\Omega}{\omega_0}$ with Ω the speed of revolution and ω_0 the eigenfrequency. Damping coefficients are $\vartheta_a = \frac{c_a}{2\omega_0 m_R}$ and $\vartheta_i = \frac{c_i}{2\omega_0 m_R}$ with internal damping c_i, outer damping c_a, and rotor mass m_R.

3.2 Jeffcott rotor with viscous internal damping in rotor shaft connection

Viscous internal damping in the connection between rotor and shaft of high speed lab centrifuges occurs when rubber elements are embedded between rotor and shaft. These rubber elements are utilized to uncouple rotor vibrations from shaft movements and to facilitate the change of rotors. Furthermore they allow self-centering with acceptable bearing forces even in presence of large unbalance loads. They can be modelled as spring damper elements between rotor and shaft.
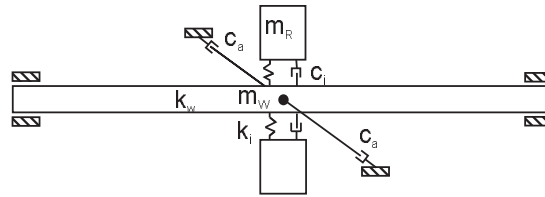

Figure 5: Jeffcott rotor with internal damping c_i, stiffness of rotor-shaft-connection k_i, shaft stiffness k_W, rotor mass m_R shaft mass m_W and outer damping c_a.

To Figure out the basic influence of stiffness, damping and mass parameters, we consider a Jeffcott rotor with one spring damper element between rotor and shaft (Figure 5). The equation of motion of the system can be written in the reference coordinate system in a non-dimensional form.

$$[M] \cdot \{x\}'' + [C] \cdot \{x\}' + [[K] + [P]] \cdot \{x\} = [0] \tag{10}$$

The matrices in equation (10) are

$$[M] = \begin{bmatrix} \rho & 0 & 0 & 0 \\ 0 & 1 & 0 & 0 \\ 0 & 0 & \rho & 0 \\ 0 & 0 & 0 & 1 \end{bmatrix}, [C] = 2 \cdot \vartheta \cdot \begin{bmatrix} 1+\varepsilon & -1 & 0 & 0 \\ -1 & 1 & 0 & 0 \\ 0 & 0 & 1+\varepsilon & -1 \\ 0 & 0 & -1 & 1 \end{bmatrix}$$

136

$$[K] = \begin{bmatrix} 1+\kappa & -1 & 0 & 0 \\ -1 & 1 & 0 & 0 \\ 0 & 0 & 1+\kappa & -1 \\ 0 & 0 & -1 & 1 \end{bmatrix}, \ [P] = 2 \cdot w \cdot \vartheta \begin{bmatrix} 0 & 0 & 1 & -1 \\ 0 & 0 & -1 & 1 \\ -1 & 1 & 0 & 0 \\ 1 & -1 & 0 & 0 \end{bmatrix}$$

The dimensionless entities are mass ratio $\rho = \frac{m_w}{m_R}$, stiffness ratio $\kappa = \frac{k_w}{k_i}$, outer damping ratio $\varepsilon = \frac{c_a}{c_i}$, $\omega_0^2 = \frac{k_i}{m_R}$, internal damping ratio $\vartheta = \frac{c_i}{2 \cdot \omega_0 \cdot m_R}$ and frequency ratio $w = \frac{\Omega}{\omega_0}$. The vector $\{x\} = \left\{ \begin{array}{cccc} x_w & x_R & y_w & y_R \end{array} \right\}^T$ contains dimensionless rotor deflections (index R) and dimensionless shaft deflections (index w).

To compute the boundary frequency which separates the stable from the unstable speed range, we first assume that there is no outer damping, that means $\varepsilon = 0$.

The stability of the equation of motion (10) can be analyzed by an extension of the Thomson and Tait theorem:

The system

$$[M] \cdot \{x\}'' + [[C] + [G]] \cdot \{x\}' + [[K] + [P]] \cdot \{x\} = [0] \tag{11}$$

is stable if $[M]$ and $[[K]+[P]]$ are symmetric and positive definite, $[C]$ is symmetric and positive semi-definite and $[G]$ is a skew-symmetric gyroscopical matrix (Müller (1977)).

Due to the terms of internal damping, the matrix $[[K] + [P]]$ is not symmetric. Therefore equation (10) should be transformed to eliminate the skew symmetric terms in matrix $[[K] + [P]]$. Following a proposal of Müller (1977) this can be done with a transformation matrix $[L]$, whereby $[L]$ fulfills the differential equation

$$[C] \cdot [L]' + [P] \cdot [L] = [0] \tag{12}$$

One obtains

$$[L] = \begin{bmatrix} [I] \cdot \cos(w\tau) & -[I] \cdot \sin(w\tau) \\ [I] \cdot \sin(w\tau) & [I] \cdot \cos(w\tau) \end{bmatrix} \tag{13}$$

with $[I]$ the unit matrix and

$$\{x\} = [L] \cdot \{\xi\} \tag{14}$$

$$\{x\}' = [L]' \cdot \{\xi\} + [L] \cdot \{\xi\}' \tag{15}$$

$$\{x\}'' = [L]'' \cdot \{\xi\} + 2 \cdot [L]' \cdot \{\xi\}' + [L] \cdot \{\xi\}''. \tag{16}$$

This yields the transformed equation of motion

$$[M^*] \cdot \{\xi\}'' + [[C^*] + [G^*]] \cdot \{\xi\}' + [K^*] \cdot \{\xi\} = [0] \tag{17}$$

with

$$[M^*] = [M], \ [C^*] = \begin{bmatrix} 2\vartheta & -2\vartheta & 0 & 0 \\ -2\vartheta & 2\vartheta & 0 & 0 \\ 0 & 0 & 2\vartheta & -2\vartheta \\ 0 & 0 & -2\vartheta & 2\vartheta \end{bmatrix}, \ [G^*] = \begin{bmatrix} 0 & 0 & 0 & 0 \\ 0 & 0 & 0 & -2w \\ 0 & 0 & 0 & 0 \\ 0 & 2w & 0 & 0 \end{bmatrix}$$

$$[K^*] = \begin{bmatrix} -\rho w^2 + 1 + \kappa & -1 & 0 & 0 \\ -1 & -w^2 + 1 & 0 & 0 \\ 0 & 0 & -\rho w^2 + 1 + \kappa & -1 \\ 0 & 0 & -1 & -w^2 + 1 \end{bmatrix}.$$

Matrix $[M^*] = [M^*]^T$ is positive definite and matrix $[C^*] = [C^*]^T$ is semi-definite. According to the above mentioned stability definition, matrix $[K^*]$ should be positive definite. For the boundary frequency follows

$$w_b = \sqrt{\Gamma - \sqrt{\Gamma^2 - \frac{\kappa}{\rho}}}, \ \Gamma = \frac{1}{2}(1 + \frac{1+\kappa}{\rho}) \tag{18}$$

The boundary frequency w_b coincides with the lower critical frequency of the system w_{crI}. The upper one is

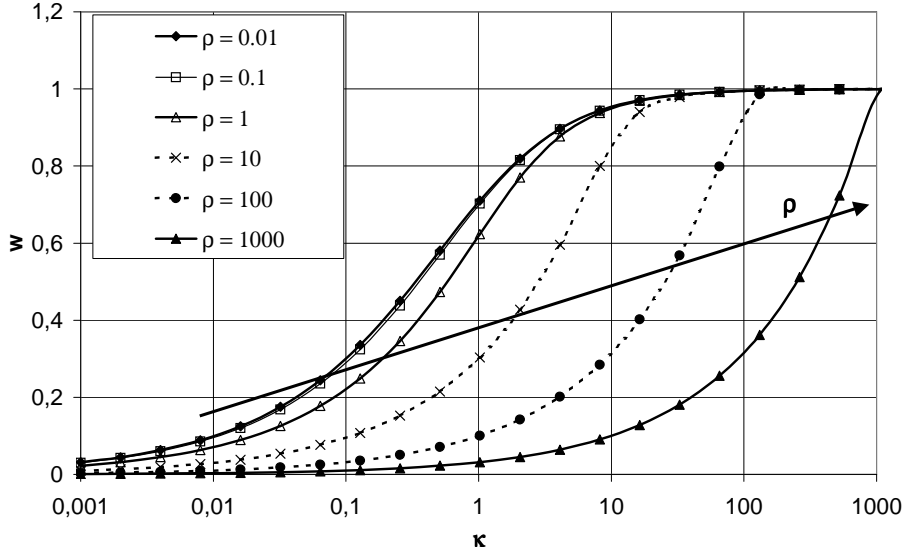$$w_{crII} = \sqrt{\Gamma + \sqrt{\Gamma^2 - \frac{\kappa}{\rho}}}. \tag{19}$$

Figure 6: Boundary frequency $w_b = \frac{\Omega}{\omega_0}$ against stiffness ratio $\kappa = \frac{k_w}{k_i}$ and mass ratio $\rho = \frac{m_w}{m_R}$.

In Figure 6 the influence of the stiffness ratio $\kappa = \frac{k_w}{k_i}$ and the mass ratio $\rho = \frac{m_w}{m_r}$ on the boundary frequency w_b is shown. For a huge stiffness ratio κ, that means a stiff shaft with respect to the rotor shaft connection, the boundary frequency converge to $w_b = 1$. In this case the boundary frequency is mainly affected by the internal spring stiffness k_i and the mass of the rotor m_R. For a small mass ratio ρ, that means a huge rotor mass with respect to the shaft, the boundary frequency converge faster to one for an increasing stiffness ratio κ. If the stiffness ratio is small, e.g., an elastic shaft, the boundary frequency becomes much smaller than one ($w_b \ll 1$).

By introducing outer damping c_a, the boundary frequency w_b can be increased. In the following it is studied in which range the system can be stabilized.

The previously used approach to transform the equation of motion such that the above mentioned stability condition of Müller (1977) can be adopted is impossible in this case. It is impossible to determine a suitable transformation matrix $[L]$ which fulfills equation (12) and the condition to be orthogonal at the same time. A matrix $[L]$ which solves equation (12) causes that the mass matrix $[M^*]$ and the stiffness matrix $[K^*]$ in the transformed equation become time-dependent.

It is possible to determine a stability range which coincides with the system with no outer damping by using the stability definition of Ljapunov. However it is not possible to find a Ljapunov function which is adequately close to show the influence of outer damping.

Applying the Hurwitz criterion to identify the boundary condition is analytically extensive. Similarly an analytical calculation of the real part of the eigenvalues gets extensive or even impossible.

Hence, the system with outer damping is evaluated numerically. Stiffness, mass, and outer damping ratio and internal damping are changed in a certain range during the calculation such that 200 different configurations are computed. For each parameter set the speed of revolution is altered step-by-step from zero to a maximum speed. Once the real part of one eigenvalue becomes positive during calculation, the previous speed step is stored as boundary frequency w_b. The calculation was performed by FERAN. Some results are shown in Figure 7.

With increasing stiffness ratio, that means with a stiffer shaft or a smaller spring stiffness between rotor and shaft, it becomes more and more difficult to enlarge the stability range by increasing the outer damping c_a (Figure 7). An increased internal damping c_i, that means an increased internal damping ratio has a negative impact on the possibility to elevate the boundary frequency by altering the outer damping (Figure 7 (left) compared to Figure 7 (right)).

Considering the simulation results it is possible to stabilize the system under certain conditions beyond the second critical speed by increasing the outer damping ratio ε.
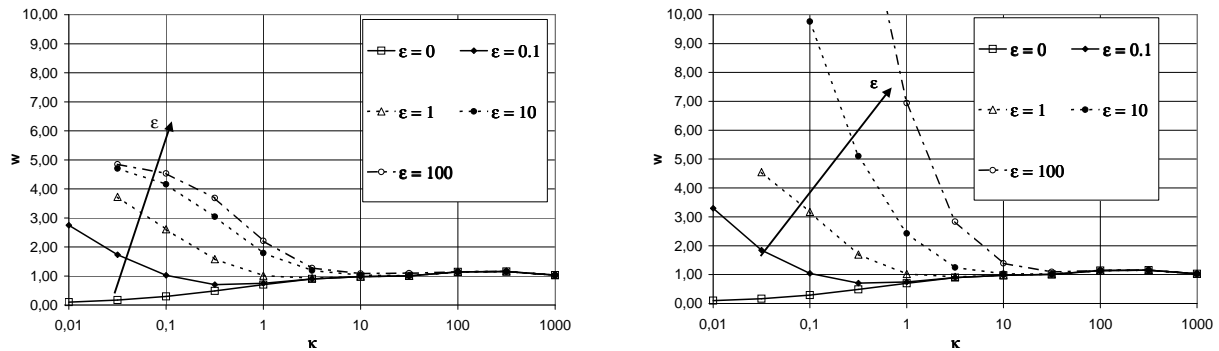
Figure 7: Effects of changing stiffness ratio $\kappa = \frac{k_w}{k_i}$ and outer damping ratio $\varepsilon = \frac{ca}{ci}$ with mass ratio $\rho = \frac{m_w}{m_R} = 0.1$. Internal damping ratio $\vartheta = \frac{c_i}{2 \cdot \omega_0 \cdot m_R} = 0.1$ on the left and $\vartheta = 0.01$ on the right.

3.3 High speed lab centrifuge with viscous internal damping in rotor shaft connection

As mentioned above, high speed lab centrifuges operate with a wide range of rotors, and the change of rotors should be as fast and easy as possible. In some cases o-ring seals are introduced in the joint of rotor and shaft to facilitate the fastening of rotors. However they produce internal damping in the rotor system. To avoid instabilities the choice of these rubber elements has to be accomplished carefully.
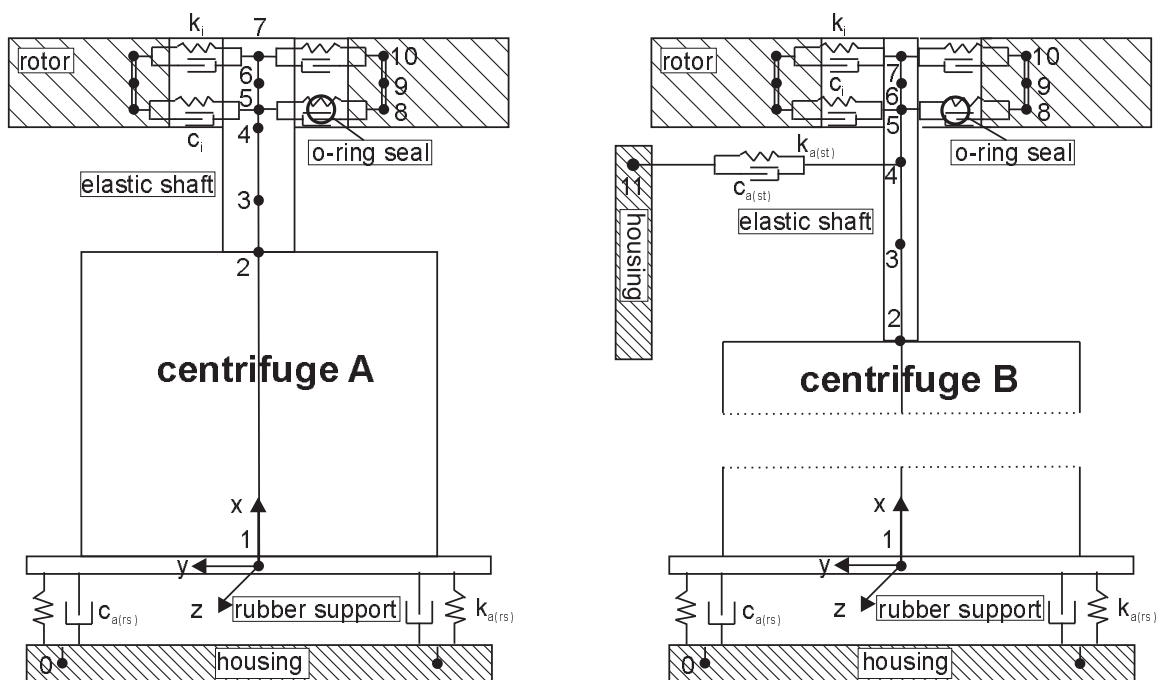

Figure 8: Models of high speed centrifuges with o-ring seals between rotor and shaft. On the left centrifuge with a short shaft (centrifuge A) and on the right with a slender shaft with an additional damper element connecting shaft and housing (centrifuge B).

3.3.1 Stabilization by outer damping

In Figure 8 left, a model of a high speed lab centrifuge with an o-ring seal coupling between rotor and shaft is shown. It should be clarified how the o-ring seals affect the stability of the system and to which extend the centrifuge could be stabilized by outer damping introduced by rubber supports.

In the simulation model of FERAN, the o-ring seals are specified by two rotating spring damper elements, acting

in translational direction (y- and z-direction). Each of them has a stiffness of $k_i = 4 \cdot 10^5 \, N/m$ and a damping of $c_i = 100 \, Ns/m$, representing the internal damping. Parameters of the rotor and the unbalance load are identical to those of the centrifuge in Section 2.6. Shaft diameters are $20 \, mm$ between node 1 and node 2, $13 \, mm$ between node 2 and node 4 and $22 \, mm$ between node 4 and 7, shaft length is $126 \, mm$, $68 \, mm$ between node 1 and 2, $25 \, mm$ between node 2 and 4 and $2.5 \, mm$ between node 4 and 5. Outer damping is introduced by the rubber support. Four simulations were conducted with different damping values of the rubber support between $c_{a(rst)} = 0 \, Ns/m$ and $c_{a(rst)} = 150 \, Ns/m$(translation) and $c_{a(rsr)} = 0 \, Nms$ and $c_{a(rsr)} = 0.12 \, Nms$(rotation). The stiffness of the rubber support remained unchanged with values $k_{rst} = 9000 \, N/m$ (translation) and $k_{rsr} = 180 \, Nm$ (rotation).
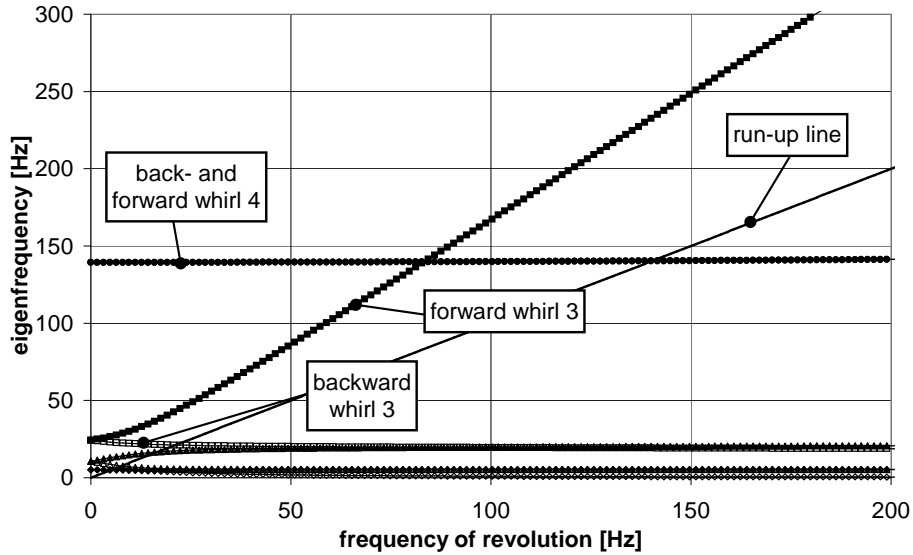

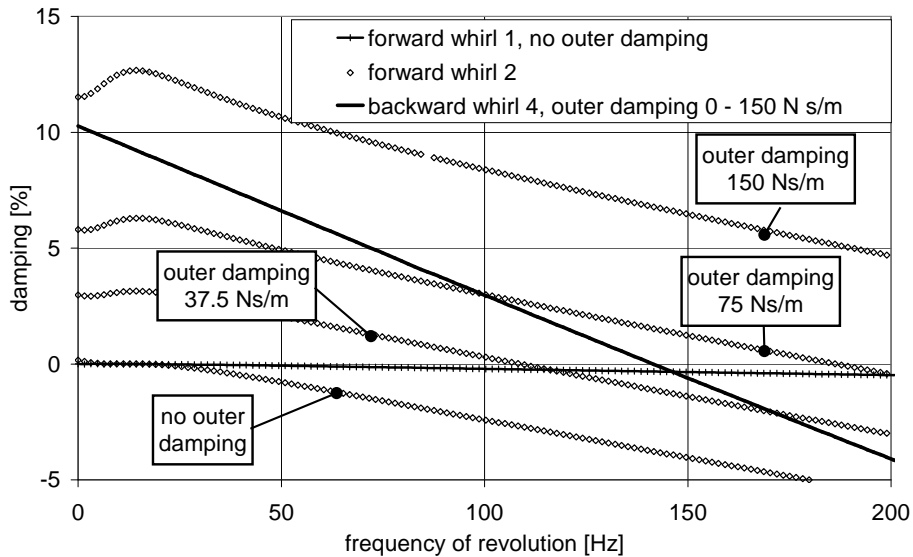Figure 9: Campbell diagram of centrifuge A.

Figure 10: Centrifuge A. Damping values of the second forward whirl and the fourth backward whirl. For the case of no outer damping, the damping of the first forward whirl is shown in addition.

In Figures 9 and 10 the Campbell diagram and damping values for different parameters of outer and internal damping are shown. If there is no outer damping, the centrifuge gets unstable above the first critical speed. For an outer damping value of $c_{a(rst)} = 37.5 \, Ns/m$, the second forward whirl gets negative at a frequency of revolution of about $110 \, Hz$. The system gets unstable. For high outer damping $c_{a(rst)} = 75 \, Ns/m$ and $c_{a(rst)} = 150 \, Ns/m$, an instability is caused by the fourth backward whirl. The damping of the fourth backward whirl remains nearly unchanged by the augmented outer damping. The damping values of the other forward and backward whirls are not shown in Figure 10 as they remain positive in this speed range. In the investigated range of outer damping

140

the damping values of the forward and backward whirls up to the third forward whirl could be increased by outer damping.

Figure 11 shows run-ups of the centrifuge. If there is no outer damping but internal damping, the system gets unstable after the first critical speed (curve (2)). The magnitudes of rotor deflection become unlimited huge. If outer damping of $c_{a(rst)} = 75\,Ns/m$ or $c_{a(rst)} = 150\,Ns/m$ is applied in addition to internal damping, the centrifuge becomes unstable beyond the third critical speed (curves (3) and (4)). The curves of both values are quiet similar. The evaluation of the centrifuge without internal damping is added for comparison (curve (1)).
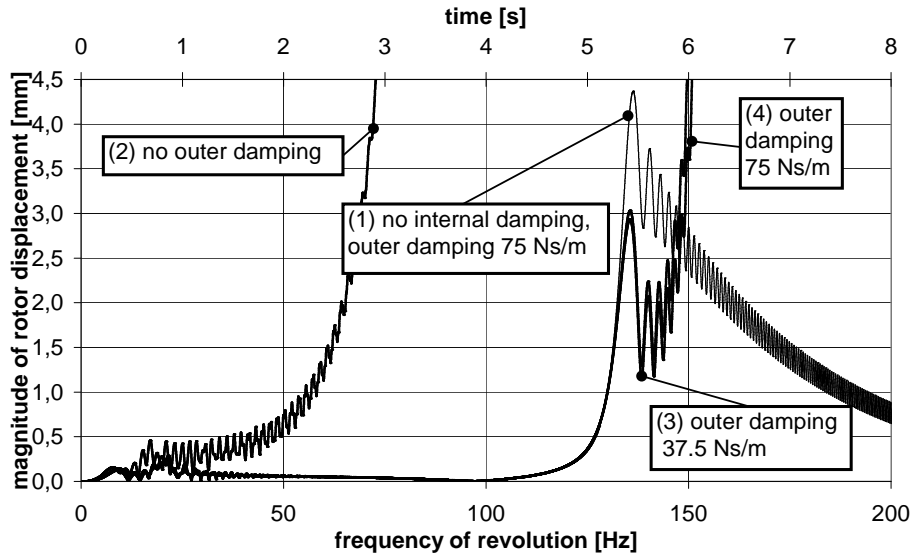

Figure 11: Centrifuge A. Run-up with internal damping (curves (2) to (4)) and without internal damping (curve (1)) for different values of outer damping.

3.3.2 Stabilization by anisotropic support

It is possible to stabilize the centrifuge in a certain manner with anisotropic bearings. To clarify the effects of anisotropic rubber support we consider the high speed centrifuge A in Figure 8 on the left for the case that no outer damping is applied. The ratio of anisotropy χ is defined as

$$\chi = \frac{k_{a(rst)y}}{k_{a(rst)z}} = \frac{k_{a(rsr)y}}{k_{a(rsr)z}} \tag{20}$$

with $k_{a(rst)y}$ stiffness of the rubber support in y-direction transverse to the shaft and $k_{a(rst)z}$ stiffness of the rubber support in z-direction transverse to the shaft, both in the initial coordinate system.

The Campbell diagram for high anisotropy ($\chi = 4$) is depicted in Figure 12. Due to the anisotropy forward and backward whirl are split even if the rotor does not rotate, see for example the third forward and backward whirl. The shape of the damping of the fourth backward whirl is not changed by increasing anisotropy (Figure 13). Only the damping of the lower forward and backward whirls can be influenced in a positive way by augmenting the anisotropy of the rubber supports stiffness. In Figure 13 only the damping curves which get negative for a frequency of revolution lower than $200\,Hz$ are shown.
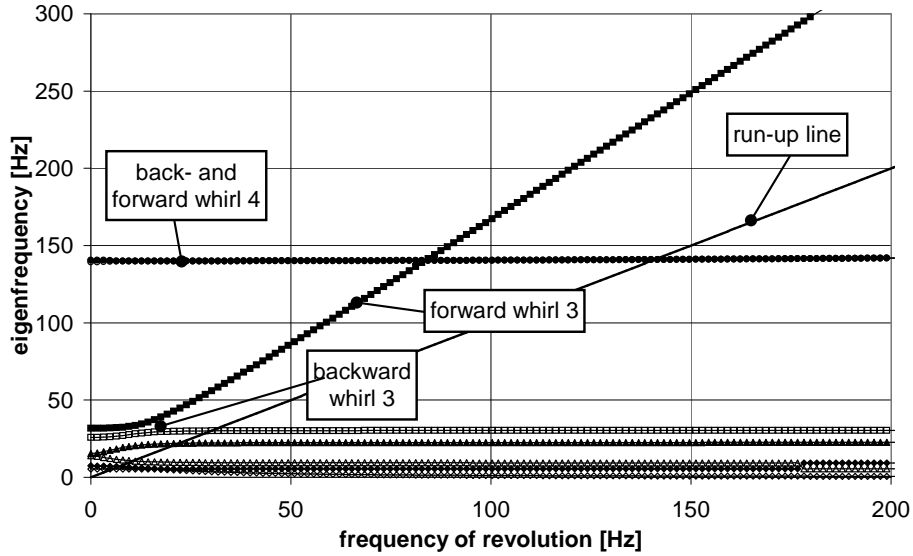
Figure 12: Centrifuge A. Campbell diagram for high support stiffness anisotropy $\chi = 4$
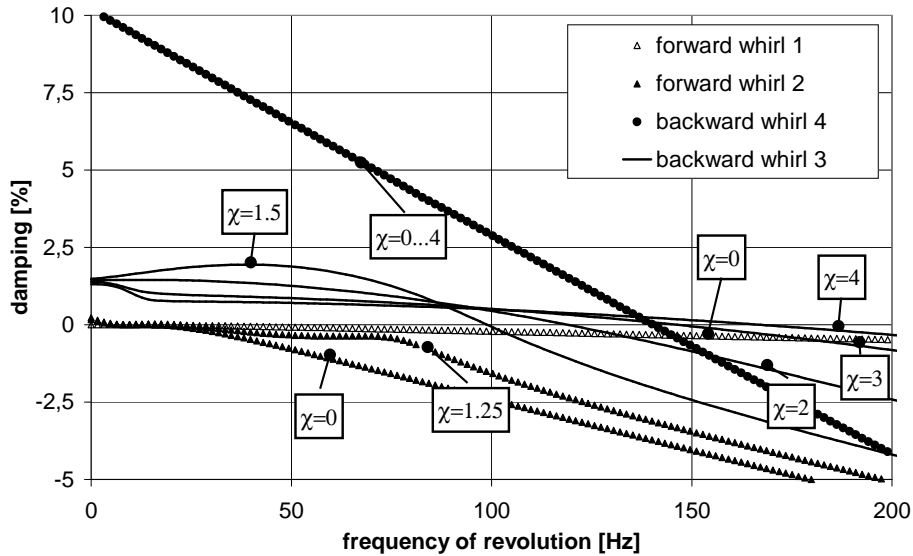

Figure 13: Centrifuge A. Damping values for different values of anisotropy χ. Only the damping curves are shown which get negative for a frequency of revolution lower than $200\,Hz$

3.3.3 Stabilization of a centrifuge with a slender shaft

In a further step we consider a high speed centrifuge with a shaft, which is more slender (Figure 8, right). This enables to mount an additional damper to the shaft close to the rotor at node 4. Shaft diameters are reduced to $6.5\,mm$ between node 2 and 5 and to $10\,mm$ between node 5 and 7, shaft length between node 2 and 5 is augmented to $50\,mm$. The stiffness of the additional damper is $k_{st} = 1000\,N/m$. Table 1 contains the damping parameters for the rubber support $c_{a(rst)}$ and $c_{a(rsr)}$, for the additional damper $c_{a(st)}$ and the distance between the lower side of the rotor (node 5) and the additional damper (node 4). Seven different sets were examined.

As the shaft gets more slender the eigenfrequencies of the fourth forward and backward whirl diminish (Figure 14). In Figure 15 damping values for set 1 are shown. The outer damping is $c_{a(rst)} = 75\,Ns/m$, $c_{a(rsr)} = 0.06\,Nms$ (rubber support) and $c_{a(st)} = 50\,Ns/m$ (additional damper).

It turns out to be possible to alter the frequency where the damping of the 3rd forward whirl gets negative by changing the damping value $c_{a(st)}$ of the additional shaft damper (set 1 compared to set 3 in Table 1). Changing the
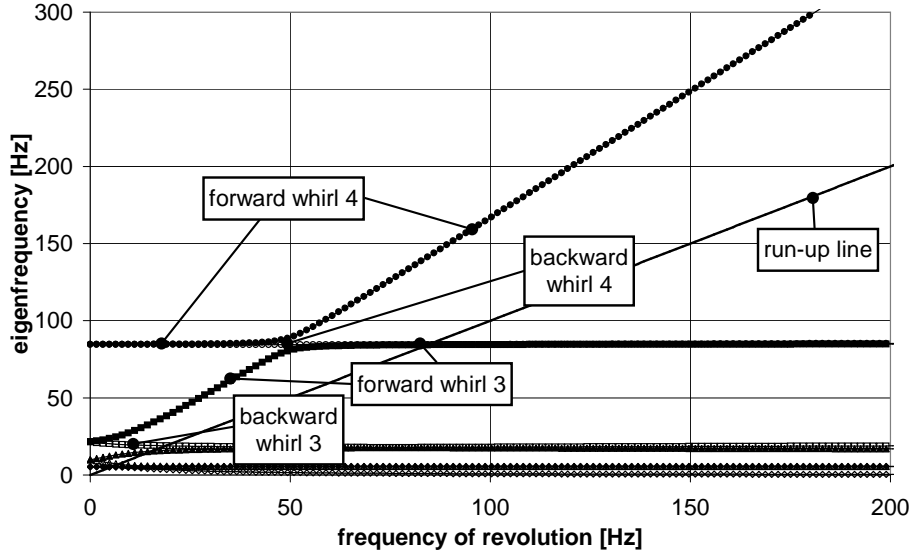
Figure 14: Centrifuge B. Campbell diagram of the centrifuge with a slender shaft.
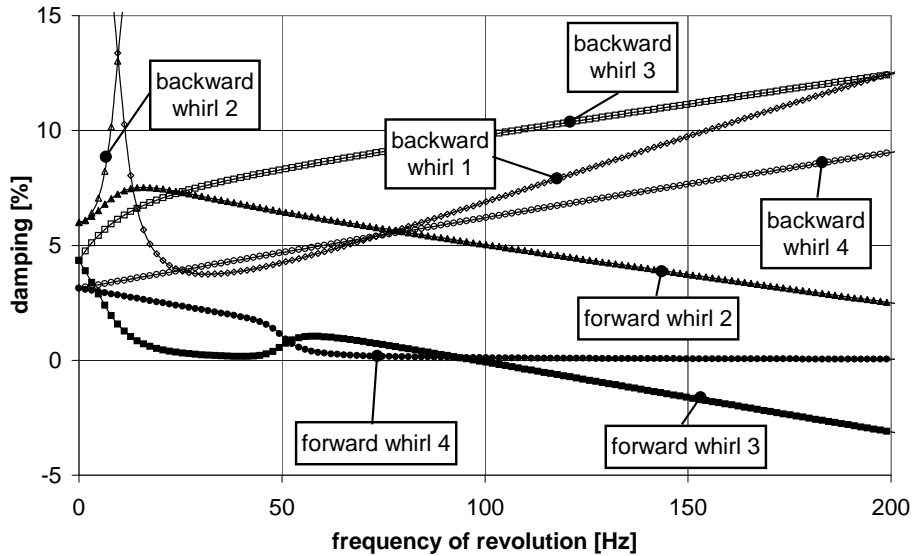

Figure 15: Centrifuge B. Damping values for $c_{a(rst)} = 75\,Ns/m$, $c_{a(rsr)} = 0.06\,Nms$ (rubber support) and $c_{a(st)} = 50\,Ns/m$ (additional damper).

damping value of the rubber support does not affect the damping of the 3rd forward whirl distinctly (set 1 compared to set 2). The distance l_{45} between the lower side of the rotor and the additional damper has an important influence to the stability range (see set 3, set 4 and set 5). Despite of its low stiffness of $k_{st} = 1000\,N/m$ the additional damper stiffens the shaft to a greater extend if its position is closer to the rotor. Similar to the results of Section 3.2 it gets more difficult to extend the stability range by outer damping (set 6 and set 7). For all seven configurations the negative damping of the 3rd forward whirl causes the instability of the centrifuge.

Considering the results of Sections 3.3.1 to 3.3.3 it is difficult to increase the damping of the fourth backward whirl respectively the third forward whirl by augmenting the damping values of the rubber support. This coincide with the simulations of the Jeffcott rotor with a stiff shaft and a weak rotor shaft connection in Section 3.2. However it is possible to influence the damping of the two lower forward whirls favorably by altering the rubber support damping or by using an anisotropic rubber support. To stabilize the third forward whirl it is convenient to introduce outer damping onto the shaft. The distance between this additional damper and the lower side of the rotor influence the stability distinctly.

	Set 1	Set 2	Set 3	Set 4	Set 5	Set 6	Set 7
$c_{a(rst)}[Ns/m]$	75	150	75	75	75	75	75
$c_{a(rsr)}[Nsm]$	0.06	0.06	0.06	0.06	0.06	0.06	0.06
$c_{a(st)}[Ns/m]$	50	50	100	100	100	100	100
$l_{45}[mm]$	15	15	15	25	35	35	15
$f_{cr}^{fw3}[Hz]$	97	97	105	120	129	91	89

Table 1: Outer damping parameters $c_{a(rst)}$, $c_{a(rsr)}$ (rubber support) and $c_{a(st)}$ (additional damper), distance between additional damper and lower side of the rotor l_{45} and frequency f_{cr}^{fw3} where damping of the third forward whirl gets negative for three different simulations.

4 Dry friction in rotor-shaft joints

If micro movements occur between rotor and shaft surface, the energy dissipation can be described by dry friction. The friction force derogates the movement of the shaft fibres. Thus an additional tension and compression of the fibres occurs, which leads to an additional force vector destabilizing the system in the post-critical speed range.

Dry friction has been investigated among others by Ishida and Yamamoto (1993). They studied nonlinear forced oscillations of a rotating shaft with nonlinear spring characteristics and internal damping via measurements and simulation. In Wettergren (2001) micro-slip and material damping in the rotor slot wedges of a turbine generator have been analyzed.

As mentioned before, an analytical description of a realistic shaft-rotor friction model is very complex and needs some assumptions.

The effects of dry friction in a rotor shaft connection of a Jeffcott rotor are investigated in the following. We consider the pressure p in the joint between rotor and shaft as non-varying during operation and not depending on the frequency of revolution. If we assume small shaft deflections $\{d\}$, the pressure p acts as a uniform load $p \cdot b_p$ on the shaft circumference, in the location of node 1 and node 3 (Figure 16). Vector $\{d\} = \{\ v(t)\quad w(t)\ \}^T$ consists of the displacements $v(t)$ and $w(t)$ transverse to the shaft direction.
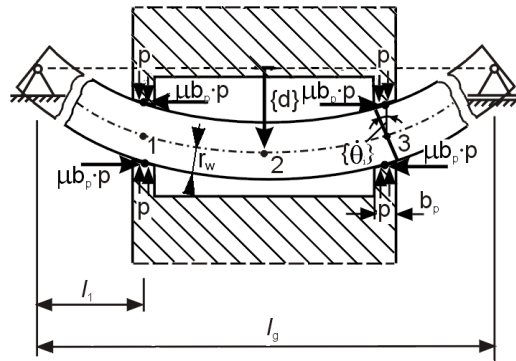

Figure 16: Model of a Jeffcott rotor with dry friction acting between shaft and rotor.

The direction of the friction force depends on the tilting speed of the shaft diameter in the rotating coordinate system $\{\dot{\theta_i}^*\}$ at node i. The friction moment of node i can be stated similar to Tondl (1965) as

$$\{M_{b\mu i}^*\} = -\kappa \cdot \frac{\{\dot{\theta_i}^*\}}{|\{\dot{\theta_i}^*\}|}. \tag{21}$$

To calculate κ we integrate the friction moment due to the load $p \cdot b_p$ at node i over the circumference of the cross section. This yields

$$\kappa = 4 \cdot \mu \cdot p \cdot b_p \cdot r_w^2. \tag{22}$$

The friction moment of each node i is transformed into the reference coordinate system:

$$\{M_{b\mu i}\} = -\frac{\kappa}{\sqrt{(\dot{\theta}_{yi} + \Omega\theta_{zi})^2 + (\dot{\theta}_{zi} - \Omega\theta_{yi})^2}} \left\{ \begin{array}{c} \dot{\theta}_{yi} + \Omega\theta_{zi} \\ \dot{\theta}_{zi} - \Omega\theta_{zi} \end{array} \right\} \tag{23}$$

The terms θ_{yi} and θ_{zi} are the inclination angles of node i in respect of y and z axes in the reference coordinate system.

Micro-movements occur when the axial force in the rotor shaft connection exceeds the friction force. To facilitate the model we suppose that the shaft movement is not affected by the rotors stiffness and geometry when rotor and shaft are connected rigidly. Furthermore, the moment M_{j1} in the joint of rotor and shaft due to the shafts bending in node 1 (Figure 16) is approximated by a function of the magnitude of the rotor deflection $|\{d\}|$ in the fixed coordinate system

$$M_{j1} = \frac{3 \cdot E \cdot |\{d\}| \cdot r_w^4 \cdot \pi}{l_g^2 \cdot |3/2\frac{l_1^2}{l_g^2} - 3/8|}. \tag{24}$$

This function is obtained applying Bernoullis beam theory. Now we can state the condition that micro movements appear

$$|M_{b\mu 1}| < |M_{j1}|. \tag{25}$$

$M_{b\mu 1}$ is the friction moment of node 1.

In Figure 17, the results of a run-up of this rotor system are shown. The magnitude of rotor displacement $|\{d\}|$ is calculated by $\sqrt{v(t)^2 + w(t)^2}$ with the displacements $v(t)$ and $w(t)$ transverse to the shaft direction. The numerical integration in FERAN was done with a modified Rosenbrock method. Parameters used for the simulation are: shaft radius $r_w = 3\,mm$, total shaft length $l_g = 180\,mm$, length $l_1 = 70\,mm$, mass of rotor $m_R = 3\,kg$, contact width per node $b_p = 2\,mm$, unbalance mass $m_u = 2\,g$, radius of unbalance $r_u = 40\,mm$, friction coefficient $\mu = 0.5$.
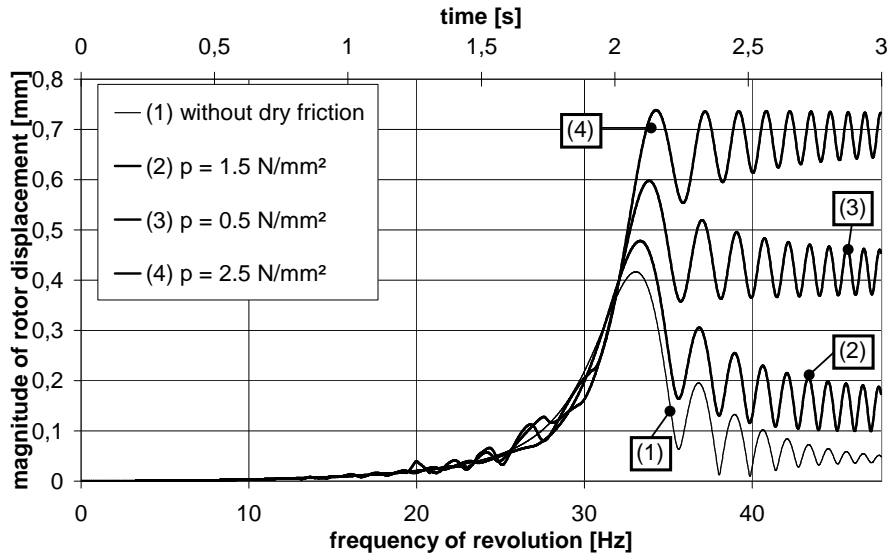

Figure 17: Run-up of a Jeffcott rotor with internal dry friction between rotor and shaft.

A dynamic simulation over the whole speed range is one way to show the effects of dry friction. After passing the first critical speed at $33Hz$, the rotor oscillates due to dry friction with the frequency of the first forward whirl added by a vibration with the frequency of revolution. As the magnitude of rotor displacement is shown one can only observe the beat frequency in the post critical frequency area which is the difference between frequency of revolution and first froward whirl.

For both cases with internal dry friction $p > 0N/mm^2$ and without internal dry friction, the beat frequency is the same, as the frequency of the first forward whirl does not change with the frequency of revolution.

Increased pressure in the shaft rotor and consequently an increased friction moment leads to higher magnitudes in the post critical frequency range provided that micro movements occur. In the subcritical speed range it is possible to Figure out the point, were micro movements start to arise due to increasing rotor deflections as the condition of equation (25) is fulfilled. Additional vibrations can be observed. The micro movements start at a higher frequency if the pressure in the rotor-shaft-connection is increased.

The higher amplitudes in the post critical speed range due to internal damping are a result of the reducing damping effects of rotating energy dissipation.

5   Conclusion

Different approaches to model internal damping are shown. With respect to viscous internal damping in rotor shaft joints it was possible to deduce an analytical formulation for the boundary frequency for a simplified rotor system with no outer damping. This model fits better to practical applications if viscous internal damping between rotor and shaft dominates and internal material damping in the shaft has a minor influence. The influence of system parameters when outer damping is applied was shown numerically.

The stability boundaries for lab centrifuges can be computed quiet well by FERAN, a rotor dynamic simulation tool, where viscous internal damping is embedded. If rotor and shaft are coupled by spring damper elements it turned out to be difficult to increase the damping of higher forward and backward whirls by augmenting the damping values of the rubber support or by using an anisotropic support. However, it is possible to influence the damping of the lower forward whirls favorably. To stabilize the higher forward and backward whirls it is convenient to introduce outer damping onto the shaft.

To describe micro movements and dry friction in the joints of shaft-rotor of lab centrifuges it is necessary to extend the simplified model of dry friction in Section 4. Measurements are necessary to Figure out the main influence parameters of dry frictions. Efforts in this direction are in preparation.

References

Cook; Malkus; Plesha; Witt: *Concepts and applications of Finite element analysis*. John Wiley & Sons, Madison, 4th edn. (2002).

Cowper: The Shear Coefficient in Timoshenko's Beam Theory. *ASME Journal of Applied Mechanics*, 33, 2, (1966), 335–340.

Feng, X.: *Nutzung Evolutionärer Strategien zur Optimierung des dynamischen Verhaltens von Laborzentrifugen*. Dissertation. Technische Universität Clausthal (2002).

Fischer, J.; Strackeljan, J.: Einsatz von Simulationstechnik zum Entwurf schnelldrehender Rotorsysteme. In: Kasper; Roland, eds., *Virtuelle Produkt- und Prozessentwicklung (7. Magdeburger Maschinenbau-Tage 11.-12. Oktober 2005). - Tagungsband*, 88 – 95, Universtität Magdeburg (2005).

Fischer, J.; Strackeljan, J.: FEM-Simulation and Stability Analyses of High Speed Rotor Systems. In: H. Springer; H. Ecker, eds., *7th International Conference on Rotor Dynamics. Conference Proceedings.*, Institut of Mechanics an Mechantronics, Vienna University of Technology (2006), paper-ID 184.

Gasch, R.; Nordmann, R.; Pfützner, H.: *Rotordynamik*. Springer Verlag, Berlin, Heidelberg, New York, 2 edn. (2002).

Hagedorn, P.; Kühl, H.; Teschner, W.: Zur Stabilität einfach besetzter Wellen mit nichtlinearer innerer Dämpfung. *Ingenieur-Archiv*, 46, (1977), 203–212.

Irretier, H.: Numerische Simulation transienter Resonanzschwingungen eines starren Rotors in spielbehafteten Lagern. In: H. Irretier; R. Nordmann; H. Springer, eds., *Schwingungen in rotierenden Maschinen*, vol. 5, 277–286, Vieweg Verlag (2001).

Ishida, Y.; Yamamoto, T.: Forced Oscillations of a Rotating Shaft with Nonlinear Spring Characteristics and Internal Damping. *Nonlinear Dynamics*, 4, (1993), 413–431.

Kellenberger, W.: Die Stabilität schnellaufender und anisotrop gelagerter Wellen mit äusserer und innerer Dämpfung. *Brown Boveri Mitteilungen*, 50, 11, (1963), 756–766.

Müller, P.: *Stabilität und Matrizen*. Springer-Verlag, Berlin, Heidelberg, New York (1977).

Ryzhik; Sperling; Duckstein: Non-Synchronous Motion Near Critical Speeds in a Single-Plane Auto-Balancing Device. *Technische Mechanik*, 24, 1.

Schäfer: *Erhöhung der Laufsicherheit schnelldrehender Rotorsysteme*. Dissertation, Technische Universität Clausthal (1994).

Schwarz: *Numerische Mathematik*. Teubner Verlag, Stuttgart (1993).

Steihaug; Wolfbrandt: An Attempt to Avoid Exact Jacobian and Nonlinear Equations in the Numerical Solution of Stiff Differential Equations. *Mathematics of Computation*, 33, 146, (1979), 521–534.

Strackeljan, J.; Feng, X.; Behr, D.: Einsatz von Evolutionären Algorithmen zur Optimierung des Laufverhaltens von schnelldrehenden Rotorsystemen. In: H. Irretier; R. Nordmann; H. Springer, eds., *Schwingungen in rotierenden Maschinen*, vol. 5, 217–224, Vieweg Verlag (2001).

Tondl, A.: *Some Problems of Rotor Dynamics*. Chapman & Hall, London (1965).

Voss, H.: Numerische Simulation, Technische Universität Hamburg-Harburg, Arbeitsbereich Mathematik (2005).

Wettergren, H.: Material and Microslip Damping in a Rotor Taking Gravity and Anisotropic Bearings Into Account. *ASME Journal of Vibration and Acoustics*, 131, (2001), 30–35.

Wilkinson; Reinsch: *Lineare Algebra*. Springer Verlag, Berlin, Heidelberg, New York (1971).

Address: Dipl.-Ing. Jonas Fischer and Prof. Dr.-Ing. habil. Jens Strackeljan, Institut für Mechanik, Otto-von-Guericke Universität Magdeburg, Universitätsplatz 2, D-39106 Magdeburg.
email: jonas.fischer@mb.uni-magdeburg.de, jens.strackeljan@mb.uni-magdeburg.de.